Enhanced Heat Transfer in Natural Convection by Means of Liquid Metals and

Partitioned Domains

By

Joel Bruce Smith

A thesis submitted in partial fulfillment
of the requirements for the degree of
Master of Science in Engineering
(Mechanical Engineering)
in the University of Michigan-Dearborn
2024

Master's Thesis Committee:

    Professor Oleg Zikanov, Chair
    Assistant Professor Hugo Casquero
    Assistant Professor Doohyun Kim

Table of Contents

List of Tables

List of Figures

List of Variables

AR – Aspect Ratio

c – Courant Coefficient

C_p – Specific Heat

D – Cylinder Diameter

g – Acceleration of Gravity

Gr – Grashof Number

H – Cylinder Height

H_g – Gap Height Above and Below Partitions

N_E – Number of Elements of Compute Grid

p – Pressure

p_b – Fluid Bulk Pressure

Pr – Prandtl Number

Ra – Rayleigh Number

Ra_{cr} – Critical Rayleigh Number

S_{TB} – Top/Bottom Cylinder Surface Area

T – Temperature

T_b – Fluid Bulk Temperature

T_{cold} – Cold Sink Surface Temperature

T_{hot} – Heat Source Surface Temperature

T_{melt} – Melting Temperature

U – Free-Fall Velocity

α – Ratio of Top and Bottom H_g

β – Coefficient of Thermal Expansion

ΔT – Temperature Difference

Δt – Time Step Size

Δx – Mesh Element Length

δ – Ratio Partition Gap and Cylinder Height

$δ_B$ – Average Thermal Boundary Layer H

$δ_{BL,lower}$ – Lower Thermal Boundary Layer H

$δ_{BL,upper}$ – Upper Thermal Boundary Layer H

φ – Angle of Applied Gravity

χ – Thermal Diffusivity

λ – Thermal Conductivity

ρ – Density

μ – Dynamic Viscosity

Θ – Angle Between x and y Magnitudes

ν – Kinematic Viscosity

Ω – Frequency

Abstract

The rate of heat generation in modern systems and components, such as larger batteries for energy storage, powerful instrumentation in computing, and advanced HVAC and climate control systems, has continued to increase in large part by inevitable technological advancement. Assuming progress continues, the research of heat transfer efficiency remains a meaningful and worthwhile endeavor. This study explores possible ways to increase the effectiveness of heat transfer by means of natural convection for a wide range of systems at relatively low temperature. It is theorized that a combination of the high energy density and high thermal conductivity of liquid metals combined with the effects of vertical partitions on flow organization in a fluid cavity can positively impact the heat transfer rate of a convective cell. This hypothesis is explored for the geometry of a cylindrical cavity with a single partition using Ansys Fluent CFD simulations. The aspect ratio of the cylinder, the Rayleigh number of the convective fluid flow, and the gap height between the top and bottom cylinder surfaces and a partition are considered factors of a parametric optimization study. The results show a manyfold enhancement of the heat transfer rate by a partition and indicate a strong potential in heat transfer applications.

1. Introduction

Rayleigh-Benard Convection (RBC), a phenomenon in which thermal stratification of a fluid within a cavity facilitates convection, can be observed improving heat transfer amongst a myriad of thermal systems both natural and man-made. This can be observed prominently in a vertically oriented thermal system circulating a working fluid such as air, water, or refrigerant. In the interest of expanding on its potential, we explore alternative configurations of RBC that may yield greater improvements in heat transfer.

Although not commonly used, liquid metals have a high specific heat and thermal conductivity, consequently having a greater heat transfer potential in comparison to common working fluid [1]. However, liquid metals have a relatively high melting point and are therefore only considered for applications at higher temperatures. To optimize heat transfer for an array of systems that operate at low temperatures, liquid gallium will be used as the working fluid in this research. Its low melting point makes it liquid at just above room temperature which is within the temperature range of typical water or air cooled systems. Moreover, data on the material properties of liquid gallium is more readily available when compared to other liquid metals and compounds. Further research into convective heat transfer improvements for RBC shows potential with the implementation of partitions in a convective cell by assisting in the organization of flow, although only observed for water and air [2], [8].

The hypothesis motivating this study is that a significant heat transfer enhancement can be achieved by combining the effects of liquid metal used as a working fluid and a partition of

the flow domain. In the following sections, background information pertaining to liquid metal convective heat transport, partitioned flow, methods used for analysis and simulation, and outcomes of the simulations and resulting data will be discussed.

1.1. Literature Review

Understanding the effects of partitioned RBC for a liquid metal flow requires comprehension of the factors affecting the heat transfer in RBC. Formation of a thermal boundary layer is expected for flows with a temperature difference between a surface and fluid flowing over it. This effect should be notable for fluids with a low Prandtl number fluid which dissipate heat quickly, such as liquid metals [11]. For simulation of a vertically mounted cylindrical convective cell, thermal boundary layers are predicted to form near the cold and hot regions of the top and bottom surfaces, respectively. Identifying these thermal boundary layers, which are a source of resistance to heat transfer, provides information on the effectiveness of RBC and how much of an effect the thermal boundary layer resistance has. There exists a plethora of research investigating methods for reducing this resistance, such as deformation of the boundary layers. In one such study, boundary layer deformation of the standing-wave type, that being a combination of two waves at the same amplitude and frequency, changes global responses to convection turbulence, given that the deforming amplitude of the standing waves is close to or larger than the boundary layer thickness of the flow in RBC [5].

The large-scale circulation caused by RBC in a convective cell also has a prominent effect on the heat rate transfer [8]. Modifying the large-scale circulation may, therefore, be used to increase the heat transfer rate. Due to a limited number of published studies on liquid metals, value can be found in works published on more common working fluids. Research from a study on large-scale circulation used empirical data produced through experimentation to study

9

different types of convective domains for modifying RBC bulk flow [4]. For two different flow domain setups, type 1 with a square grid suspended in a convective cell and type 2 with the grid fully extending to the top and bottoms of the convective cell, heat transfer efficiency within the type 1 domain was enhanced by up to 14%. It was suggested that increased plume coherency caused this effect. Furthermore, heat transfer efficiency in the type 2 domain, with longer segments or "sub-units" of flow, increased by as much as 30%. These results confirm that the organization of the flow is a component of heat transfer optimization.

Geometry and orientation of the convective cell cavity play a significant factor in RBC heat transfer. For a cylinder, the ratio of the height to diameter, known as the aspect ratio AR, influences RBC by defining the shape in which flow can occur. Research suggests an increase in heat transfer can be observed in convective cells with a lower AR, caused by modification of large-scale circulation. In a confined geometry, the amount and intensity of hot and cold plume clusters increases and are more energetic, which has a significant influence in reducing the thickness of the thermal boundary layers [6]. However, the organization of the flow aided by the partitions may facilitate increased heat transfer even with an increase in the surface area of a taller convective cell of the same diameter. Additionally, the effect of a smaller convective cell must also be noted, which leads to a decrease in the volume of fluid and thus reduces the amount of heat transport that can be accommodated.

Looking at the effects of just the partitions on the convective cell geometry shows promise for improved heat transfer. Partitioned RBC may lead to reduction of heat exchange between hot ascending and cold descending jets which reduce heat transfer [5], [7]. Further research shows that adding vertical partitions in a convective cell with a high-Prandtl number liquid increases convective heat transfer in a liquid medium by increasing Nu when compared to

10

non-partitioned cases [2]. Investigation of the causes of this increase suggests that partitions in a large-scale circular fluid flow within a fluid cavity create a symmetry-breaking bifurcation, causing the fluid to organize into a unidirectional flow along the partition walls. This can create a disruption of the thermal boundary layer where the partitions extend close to the top and bottom walls [2], [8]. Furthermore, it has been observed that mean velocity and temperature fields are correlated due to the increased coherency of the flow as number of partitions increases, leading to a meaningful, albeit small, improvement in heat flux. It should be noted that as the number of partitions increases, the volume of fluid within the cell decreases and impedance from the no-slip condition of the partitioned walls increases. Adding volume to the convective cell to compensate for the loss of working fluid may prove to negate these effects.
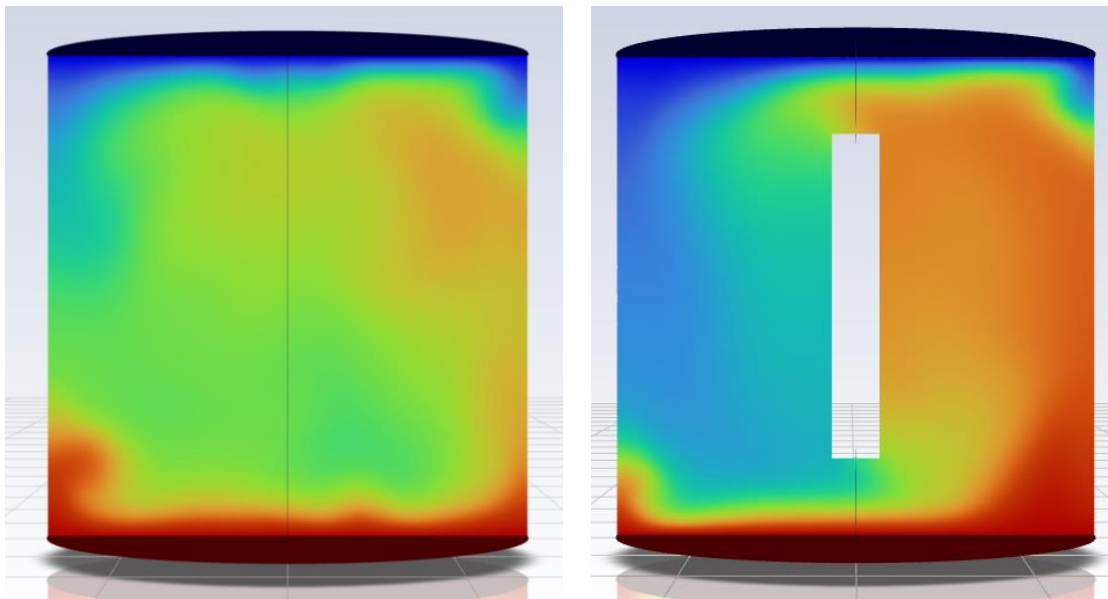

Figure 1. Simulation results of the temperature distributions for Ra=10^6, AR=1 which are discussed in detail in section 3. Instantaneous distributions of temperature in the vertical cross-section are shown. Left: RBC in a convective cell without a partition showing the typical flow organization. Right: RBC in a partitioned convective cell for δ=0.16 demonstrating stronger and more coherent large-scale circulation.

11

Additional investigation into the effects of partitions on a convective cell should yield an optimized configuration for increased convective heat transfer. It has been observed that the Nusselt number increases monotonically as the number of partitions aligned perpendicularly in a convective cell increase [2]. Aided by the partitions, the working fluid is forced through the gaps at the top and bottom of the partitions and leads to a pressure distribution at the gaps that sustain flow, creating horizontal jets, which will sweep the thermal boundary layer, disturbing these layers and further increase thermal efficiency [2]. The size of the gap height also influences the fluid flow and heat transport and may influence the flow in relation to the cell height [7].

There are several challenges when looking at generating valuable data for liquid metal flows. Liquid metals are opaque, and so measuring velocity using optical techniques, such as PIV, is impossible. What is more, systems using liquid metal tend to operate at much higher temperatures than conventional liquids such as air or water, creating difficult working conditions and energy requirements [1]. Regardless, an advantage of liquid metals that cannot be overlooked is their high thermal conductivity that facilitates more heat transfer.

It must be stressed that the effect of partitions on heat transfer in RBC is, while evident, not very strong in conventional fluids such as water. Increase of the Nusselt number by up to 30% is reported in [2], [7], [8]. As we will see in the discussion of the results in section 3, the effect is much stronger in fluids with low Prandtl numbers, e.g. liquid metals.

Understanding the advantages of partitioned RBC provides evidence that an optimized AR for increased RBC, in combination with a specific number of partitions with a given gap height, can be used to design a fluid model for which heat transfer can be optimized. It is expected that the high thermal conductivity and low viscosity of the liquid gallium should further add to optimized heat transport, outweighing the possibility of reduced heat transfer from fluid

volume reduction and increased surface area the partition will add. Thus, this thesis will report

on simulations combining the effects of liquid metal and partitioned flow in a convective cell.

2. Methods

This section will detail methods used to set up and verify the accuracy of simulations. The results will be reported and discussed in section 3.

2.1. Governing Equations and Physical Parameters

An unsteady three dimensional flow in a partitioned cylindrical cavity acting as a convective cell is calculated. Several assumptions are made to simplify the model. The Oberbeck-Boussinesq approximation is assumed in which all physical properties of the fluid are assumed constant except density in the gravity force term. Density in this case is assumed to be a linear function of temperature, thus providing the buoyant force effect. The sidewalls and the wall of the partition are assumed adiabatic with heat transfer only occurring at the top and bottom walls of the cell. No-slip boundary conditions are assumed at the walls of the cavity and along the partition walls. Under these conditions, with the cylinder height H, free-fall velocity $U \equiv \sqrt{g\beta\Delta T\,H}$, and ΔT as the typical scales, flow within the cavity can be represented by the governing equations:

$$\nabla \cdot \mathbf{u} = 0 \tag{1}$$

$$\frac{\partial \bar{\mathbf{u}}}{\partial t} + (\mathbf{u} \cdot \nabla)\mathbf{u} = -\nabla p + \Pr^{\frac{1}{2}} Ra^{-\frac{1}{2}} \nabla^2 \mathbf{u} + T\mathbf{e}_z \tag{2}$$

$$\frac{\partial T}{\partial t} + \mathbf{u} \cdot \nabla T = (RaPr)^{-1/2} \nabla^2 T \tag{3}$$

With boundary conditions

Top Surface: $z = 1,\ \ T = T_2$ Bottom Surface: $z = 0,\ \ T = T_1$

Cylinder Side Wall: $r = \frac{1}{2AR},\ \ \frac{\partial T}{\partial r} = 0$ Partition Walls: $\frac{\partial T}{\partial r} = 0$
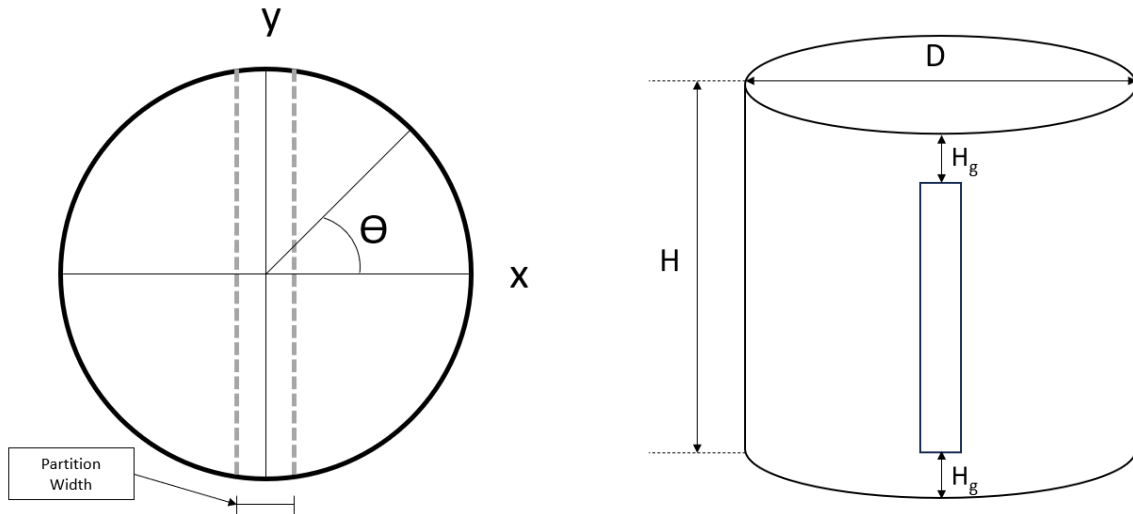

Figure 2. Geometry of the convective cell. Left: Top-down cross section of the center of the convective cell. Right: Front facing perspective of the convective cell.

The control parameters for this model are the Rayleigh number Ra, the aspect ratio of the cylinder AR, and the ratio of the partition gap height to the cylinder height δ. A change in the rate of heat transfer is anticipated by modifying AR of the convective cell cylinder, a second parameter identified as the ratio of the gap height H_g between the partition fixed to the center of the cylinder δ, and the Ra. While AR and δ are directly correlated to the model geometry, Ra and the Prandtl number Pr (ratio of kinematic viscosity to thermal diffusivity) represent design parameters determined by the properties of the fluid and the temperature difference $\Delta T = T_1 - T_2$. Specifically, Ra is the relationship between the Grashof Number Gr (ratio of buoyant force to

viscous force) and the Prandtl number Pr. A relationship between these properties and the design

parameters is shown in (1) and (2). H is the characteristic length represented by the height of the

cylinder, D is the cylinder diameter, g is the acceleration of gravity, T_{hot} is the heat source

temperature along the bottom surface, and T_{cold} is the fluid bulk temperature.

Material Properties	
T_{melt}	302.95 K
χ	1.2×10^{-5} m^2/s
β	1.2×10^{-4} K^{-1}
λ	30 W/m*K
ρ	6040 kg/m^3
ν	3.0×10^{-7} m^2/s
μ	1.81×10^{-3} kg/m·s

Table 1. Material properties of liquid gallium at 60°C [9]. Properties listed are as follows:

melting temperature T_{melt}, thermal diffusivity χ, coefficient of thermal expansion β, thermal

conductivity λ, density ρ, kinematic viscosity ν, and dynamic viscosity μ.

$$\text{Ra} = \frac{g\,\beta(T_{hot} - T_{cold})H^3}{\chi\upsilon}, \qquad \text{AR} = \frac{D}{H}, \qquad \delta = \frac{H_g}{H}, \qquad \text{Pr} = \frac{\nu}{\chi} \qquad (4)$$

$$\text{Ra} = \text{Gr} * \text{Pr} \qquad (5)$$

Research from section 1.1 is used to develop the modeled environment for simulation of

partitioned RBC with liquid gallium, the properties for which are listed in Table 1. The work

presented in this thesis is limited to the case of a single partition. The effect of multiple partitions

is left to future studies. It is anticipated that the actual width of the partition will have minimal

effects on the model assuming the partition width remains thin, and so the width of the partition

will be kept at a constant value of 10% of H for each model.

In a fully developed flow, the heat fluxes through the top and bottom walls fluctuate around the same constant mean Q_{conv}. This value is produced by averaging instantaneous values of $Q_{conv,inst}$ in time over a long period of evolution of fully developed flow. Q_{conv} is then calculated using (6) and is then used to calculate the Nusselt number Nu in (8). This value represents the ratio of convective over conductive heat transfer. Conductive heat transfer Q_{cond} will be calculated for each simulation using (7) which is a function of the cylinder height, temperature difference, and fluid properties. Higher values for Nu indicate increased convection, indicating which models produce better results for convective efficiency.

$$Q_{conv} = \frac{Q_{conv,inst}}{N_T} \qquad (6)$$

$$Q_{cond} = \frac{\lambda S_{TB} \Delta T}{H} \qquad (7)$$

$$Nu = \frac{Q_{conv}}{Q_{cond}} \qquad (8)$$

2.2. Approach to Simulations

As described below, the problem is solved computationally using Ansys Fluent, which requires the problem to be presented in dimensional units. The dimensional parameters are found for a given set of AR and Ra by fixing the temperature difference between the hot and cold surfaces ΔT and using the physical properties of gallium reported in table 1. Values for H, D, and H_g are then calculated, which provides the desired values of AR, Ra, and δ. Simulations are carried out for Ra=10^6, 10^7 and AR=1, 2, 3, 5 and the partition gaps for δ=0.04, 0.06, 0.08, 0.10. This creates a minimum of five simulations for each combination of Ra and AR, including the non-partitioned cases. The goal of the simulations is to determine for each combination of AR and Ra, which values of δ produces the greatest heat transfer, resulting in the highest value for

Nu. Additional simulations for higher or lower δ are run in case a local maximum is not found within the initial simulation set.

Beginning with the DesignModeler in Ansys, the geometry is built according to calculated values for H and D. The geometry is then meshed using the verified refined meshes discussed in Section 2.3. Setup for the simulations is done by setting a double precision and assigning CPUs. The number of CPUs per simulation is set based on the number of mesh elements, using an approximation of 1 CPU per 100,000 elements needed.

Ansys Fluent is capable of both pressure and density based solvers. These models will be run with a pressure-based transient solver due to the incompressible nature of liquid metal fluid flow and account for the change in flow over time from turbulent to fully developed flows. Model parameters are then set within the simulation by inputting the materials properties for gallium listed in Table 1, setting the flow to laminar, and having the energy equation turned on. The convective cell boundaries are set at temperatures of T_{cold}=323.15K and T_{hot}=363.15K for the top and bottom surfaces, respectively, giving a value for ΔT=40K. T_{cold} and T_{hot} are nondimensionalized by the initial bulk temperature of the fluid T_b=343.15K, giving a nondimensional temperature range of $0.94 \leq T \leq 1.06$. The initial conditions are the distribution of temperature and vertical velocity represented by (9) and (10), respectively.

$$u_z(x, y) = -(x^2 + y^2) + \frac{D^2}{4} \tag{9}$$

$$T(z) = T_{hot} + \left(-\frac{\Delta T}{H}\right) \cdot z \tag{10}$$

The flow evolution is computed with the time step $\Delta t=0.1$s and up to 200 iterations performed per Δt. The simulations fully developed flows used for final data acquisition run for a minimum of 100s. This period is increased as needed to ensure convergence of the computed statistical means to a steady value (see Figure 4). The data collected are graphed for Q_{conv} at the top and bottom surfaces and values recorded before $\Delta t=40$s ignored when calculating Nu to account for the transient nature of the initial flow profile.

2.3. Model Verification

Before partitioned models are simulated, an initial non-partitioned model is run, and the resulting data is compared to verified data of RBC at high-resolution simulations of RBC in an inclined cylinder with low Pr [3]. The non-dimensional parameters are set at Ra=10^6 and Pr=0.1, matching the non-dimensional values in the referenced study.

The geometry is built using calculated dimensions H and D and is then meshed with number of elements $N_E=130,000$ using hexahedrons as the element type. Quality of the mesh is maintained by keeping the element aspect ratio below 6. These simulations are run at $\Delta T=10$K and at varying angles between applied gravity and the z axis of the cylinder φ between 0 and 0.3π for comparison to the referenced study [3].

These verification simulations are run at only 40 iterations for time steps Δt of 0.1s. Collected data are averaged over a minimum time of 3s after steady state convergence is reached. The resulting Q_{conv} is used to calculate Nu, which is then compared to results of [3]. These calculations show excellent qualitative agreement with Q_{conv} increasing with φ as predicted in [3]. The quantitative agreement is within 5% shown in Table 2.

φ	0	0.1π	0.2π	0.3π
$Nu_{[3]}$	7.25	8.10	8.50	8.70
$Nu_{[This\ Study]}$	7.15	8.40	8.91	9.06
Percent Error	1.3%	3.5%	4.6%	3.9%

Table 2. Percent errors for Nu values in an incline cylinder between simulated results and the

data of high resolutions [3].

2.4. Grid Sensitivity Study

Additional testing of this model is performed to determine mesh independence, ensuring that values for heat transfer are only a function of the flow parameters and not of the mesh parameters. This sensitivity study will ultimately determine the element size, number of elements N_E, and element type which will provide accurate results. First, the simulation of a flow in a non-partition cavity is run at Ra=10^5 and AR=1 for meshes with hexahedron elements at N_E=133,104 and tetrahedral element meshes at N_E=133,326. Increased mesh density spanning a distance from the top and bottom surfaces at approximately 5mm is included for both models to account for the increased activity near the thermal boundary layers. Nu is then calculated as mentioned in Section 2.1, using the time average values of the instantaneous temperatures where both models reach a fully developed flow, this being after 600 time steps, and using (6), (7), and (8). Values of Nu for the hexahedron and tetrahedral models are found to be Nu=3.25 and Nu=3.23, respectively. This gives a percentage error of less than 1% and validates that the tetrahedral elements can be used in place of hexahedron elements. Although hexahedron elements can provide improved accuracy with less elements, tetrahedral elements are better for complex geometry which will be a factor once adding the partition to the model. Therefore, further meshing will be done with the tetrahedral elements.

Finding the minimum mesh resolution that provides a reasonably accurate solution is determined by running multiple tests of a non-partitioned models at Ra=10^6, AR=1 and a partitioned model at Ra=10^7, AR=3, δ=0.016 both with increasing N_E. The accuracy is determined by finding the point at which the value of Nu change minimally as N_E changes. As can be seen in Figure 3, Nu decreases as the resolution increases, with Nu starting to level out at approximately N_E=1.4 million elements. This number is taken as acceptable in providing sufficient accuracy for the purposes of this study. Anticipated increased activity in and around the thermal boundary layers near the top and bottom surfaces requires a higher mesh resolution, which can be seen in Figure 5. This increased resolution is especially important when adding the partition which falls within the thermal boundary for each partitioned model.

The accuracy of the numerical model used in the study is further analyzed by using the computed maximum velocity found to calculate the Courant Coefficient c. The coefficient is used to determine the stability of schemes for hyperbolic equations and establishes the distance to which information is transported by velocity over a time step in relation to the mesh step [10]. Explicit schemes for purely hyperbolic equations are generally stable if the Courant-Friedrichs-Lewy stability condition (11) is met. Ansys simulations use an implicit scheme which can be considered stable even when the condition is not met, the values for which are listed in Table 3.

$$c = |u_{max}|\frac{\Delta t}{\Delta x_{min}} \leq 1 \qquad (11)$$

Nondimensional Parameter Combinations at N ~ 1.4 Million	Instantaneous Max Velocity (m/s)	Mesh Length at Max Velocity (m)	C (Δt=0.1s)
Ra=10^6 AR=1 No Partition	3.72E-2	1.50E-4	24.8
Ra=10^7 AR=3 δ=0.016	1.59E-1	4.15E-4	38.3

Table 3. Courant coefficients c calculated for further mesh verification.

Number of Elements	Nu for Ra=10^6	Nu for Ra=10^7
2900000	6.25	-
2230000	6.27	6.99
2000000	-	7.01
1350000	-	7.05
1200000	6.28	-
1060000		7.17
750000	6.37	-
690000	-	7.37
345000	-	7.58
80000	-	8.09

Table 4. Values of Nu as a function of N_E which is represented graphically in Figure 3.
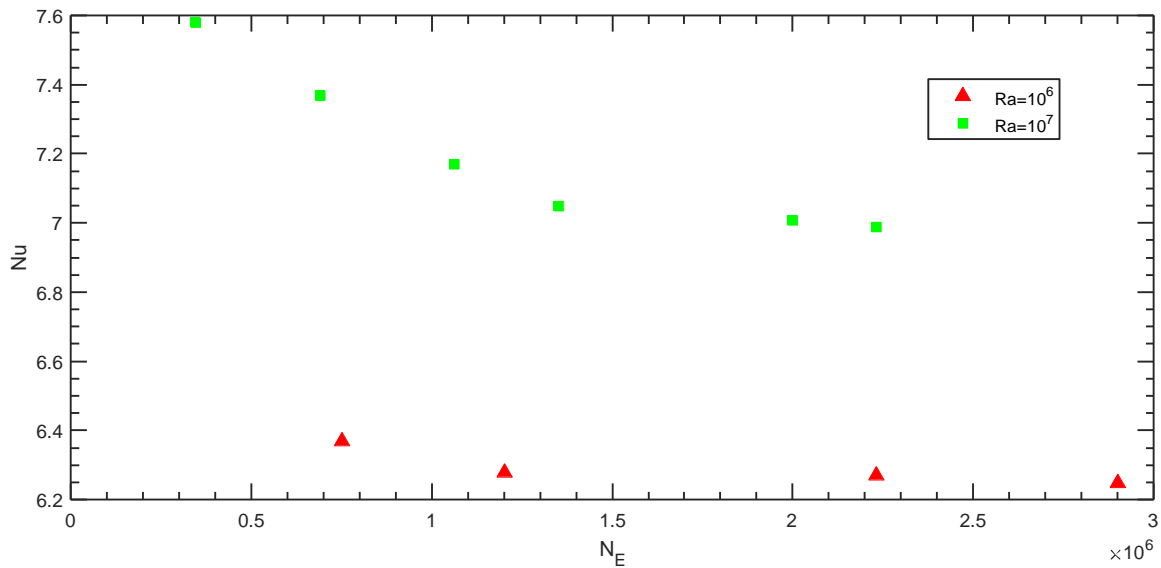

Figure 3. Nu as a function of number of elements N. Results are shown for the non-partitioned domain at Ra=10^6 AR=1 (red) and partitioned domain at Ra=10^7 AR=3 δ=0.016 (green).

It should be noted that implicit schemes are unconditionally stable but have a truncation error heavily influenced by numerical dissipation; this can result in the amplification of a rounding error. To mitigate this effect, further simulations continue with a small time step size at 0.1s. These verifications lead to the final design parameters for data collection simulations.

2.5. Simulation Procedure

Each model geometry is built using values for H based on set combinations of the non-dimensional parameters Ra and AR. A non-partitioned case is first run to find a baseline value for the heat transfer at the top and bottom of the cells and calculate Nu_0. Instantaneous velocities along the z-axis in each non-partitioned simulation are collected and averaged over time to establish upper and lower thermal boundary layer thicknesses $\delta_{BL,upper}$ and $\delta_{BL,upper}$.

$$\delta_{BL,lower} \equiv (T_b - T_{hot}) \left|\frac{dT}{dz}\right|^{-1}_{z=0} \tag{12}$$

$$\delta_{BL,upper} \equiv (T_b - T_{cold}) \left|\frac{dT}{dz}\right|^{-1}_{z=H} \tag{13}$$

Where T_b is the bulk temperature of the fluid outside of the boundary layer. The models for partitioned domains are then built for δ=0.04, 0.06, 0.08, and 0.10. If a local maximum of Q_{conv} is not found in these simulations, models for additional values for δ are built and simulated.
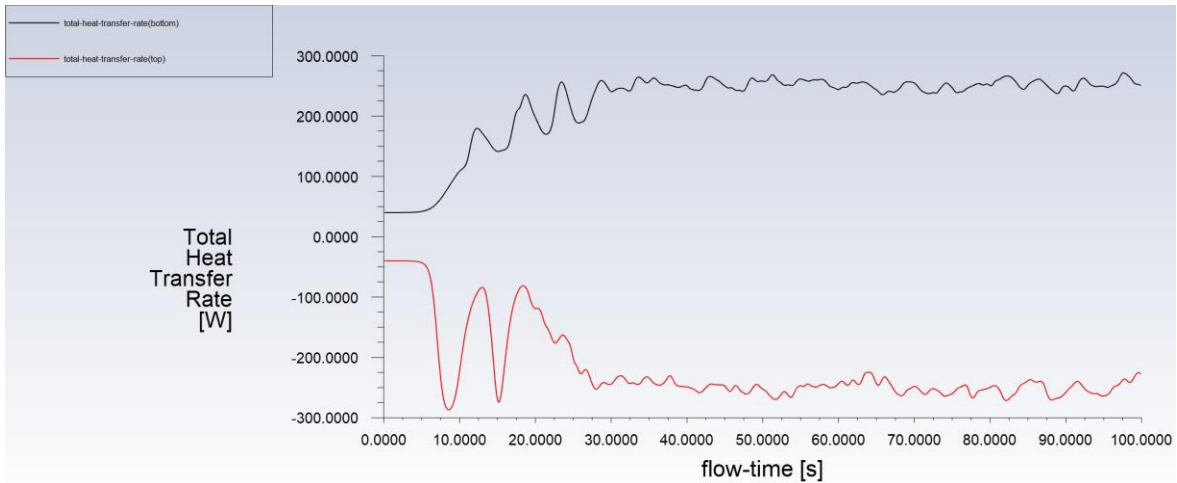
Figure 4. Graph for the total rate of heat transfer at the top and bottom of the cell during the entire simulation for Ra=10^6 AR=1. The trend over time shows convergence of the heat transfer rate at both top and bottom walls to approximately 275W.
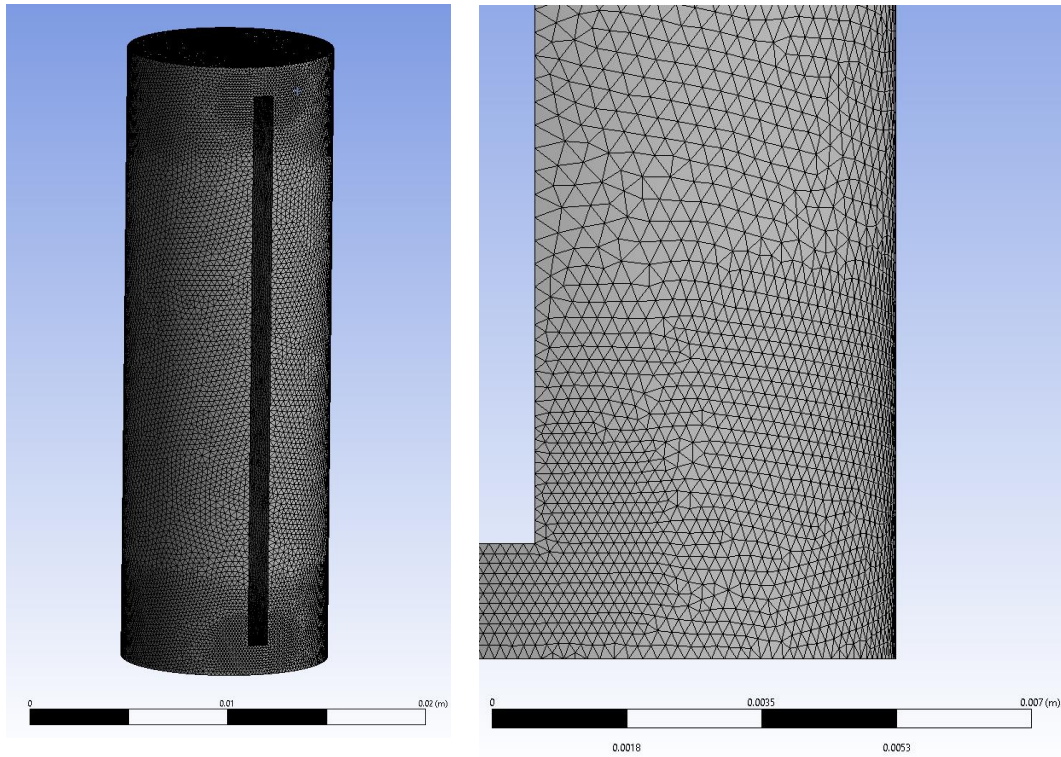
Figure 5. Zoomed in region of the mesh at the partition gap showing increased mesh resolution

within the thermal boundary layers near the top and bottom surfaces.

3. Results and Discussion

3.1. Effect of Partition on Heat Transfer

The main results of the study are summarized in Table 5, showing all but two simulations presenting a notable increase in Nu over the non-partitioned counterparts, the exceptions being $\delta=0.04$ and $\delta=0.06$ for Ra=10^6 AR=1. A value of δ was found for each combination of Ra and AR which produced the highest Nusselt number δ_{max}, resulting in the greatest convective heat transfer amplification.

The data in table 5 present a trend in which δ_{max} decreases as AR increases, which is further decreased with an increase in Ra as shown in Figure 7. This demonstrates an inverse relationship between δ and combinations of AR and Ra.

Ra	10^6				10^7			
AR	1	2	3	5	1	2	3	5
No Partition	6.28	4.98	3.06	1.00	10.5	9.28	7.92	4.65
δ=0.01	-	-	-	-	-	-	-	17.45
δ=0.02	-	-	-	10.91	-	-	18.69	**25.65**
δ=0.04	5.77	7.86	11.07	**13.05**	12.40	17.08	**21.33**	25.25
δ=0.06	6.20	9.32	**11.49**	11.40	12.50	**17.66**	19.32	20.60
δ=0.08	6.40	**9.86**	10.56	9.65	**12.80**	16.98	17.91	19.15
δ=0.10	6.80	9.56	9.57	8.35	11.80	16.38	16.38	17.70
δ=0.12	6.83	-	-	-	-	-	-	-
δ=0.14	**6.90**	-	-	-	-	-	-	-
δ=0.16	6.78	-	-	-	-	-	-	-

Table 5. Time-averaged values of Nu computed in all completed simulation.

Ra	10^6				10^7			
AR	1	2	3	5	1	2	3	5
δ=0.01	-	-	-	-	-	-	-	3.75
δ=0.02	-	-	-	10.90	-	-	2.36	5.51
δ=0.04	0.92	1.00	3.62	13.10	1.18	1.84	2.69	5.43
δ=0.06	0.98	1.19	3.75	11.05	1.19	1.90	2.44	4.43
δ=0.08	1.02	1.26	3.45	9.65	1.21	1.83	2.26	4.12
δ=0.10	1.08	1.22	3.13	8.35	1.12	1.77	2.07	3.81
δ=0.12	1.09	-	-	-	-	-	-	-
δ=0.14	1.10	-	-	-	-	-	-	-
δ=0.16	1.08	-	-	-	-	-	-	-

Table 6. Normalized values of the Nusselt Number (Nu/Nu_0).
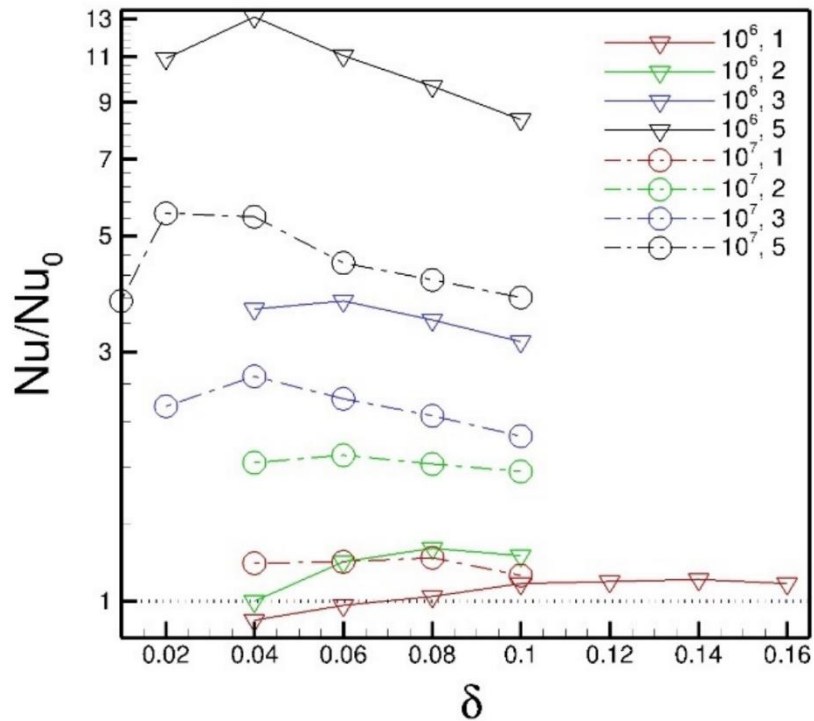
Figure 6. Graphical Representations of normalized values for the Nusselt Number.

This trend stays consistent with the data for the Nusselt number of partitioned models normalized with the Nusselt number for non-partitioned models Nu/Nu_0, shown in Figure 6. This figure also shows that higher values of Nu are produced for AR≤2 at Ra=10^7 and for AR≥3 at Ra=10^6, presenting a relationship between AR and Ra that can be observed in Figure 7.
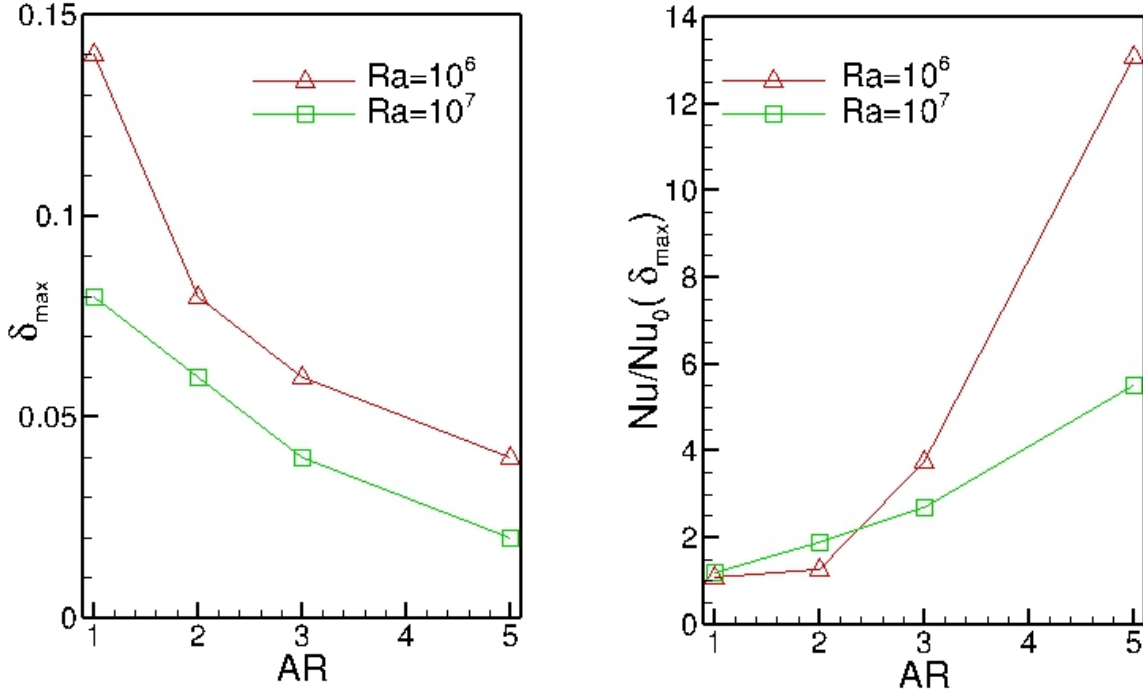
Figure 7. Left: Graphical representation of the inverse relationship between δ_{max} and combinations of Ra and AR. Right: Normalized values of Nu at δ_{max} as a function of Ra and AR showing a direct relationship that becomes more extreme as Ra decreases.

3.2. Effect of Partition on Flow Structure

Figures 8a through 15g present the flow structure and discuss the results based on temperature profiles with a nondimensional range of $T = 0.94$ (blue) to $T = 1.06$ (red). The partition created changes in the flow structure in two significant ways. First, it can be observed that adding the partition creates the large-scale circulation of the flow, which was noted to influence heat transfer when modified [8]. Second, having δ smaller than the thermal boundary layer leads to an increased heat flux by intensifying the heat transfer across the thermal boundary layer. However, a decrease of δ also has a detrimental effect on heat transfer, because a small gap creates obstruction to the flow which reduces its kinetic energy. The relation between δ and the thickness of the thermal boundary layer is further discussed in section 3.3.

27
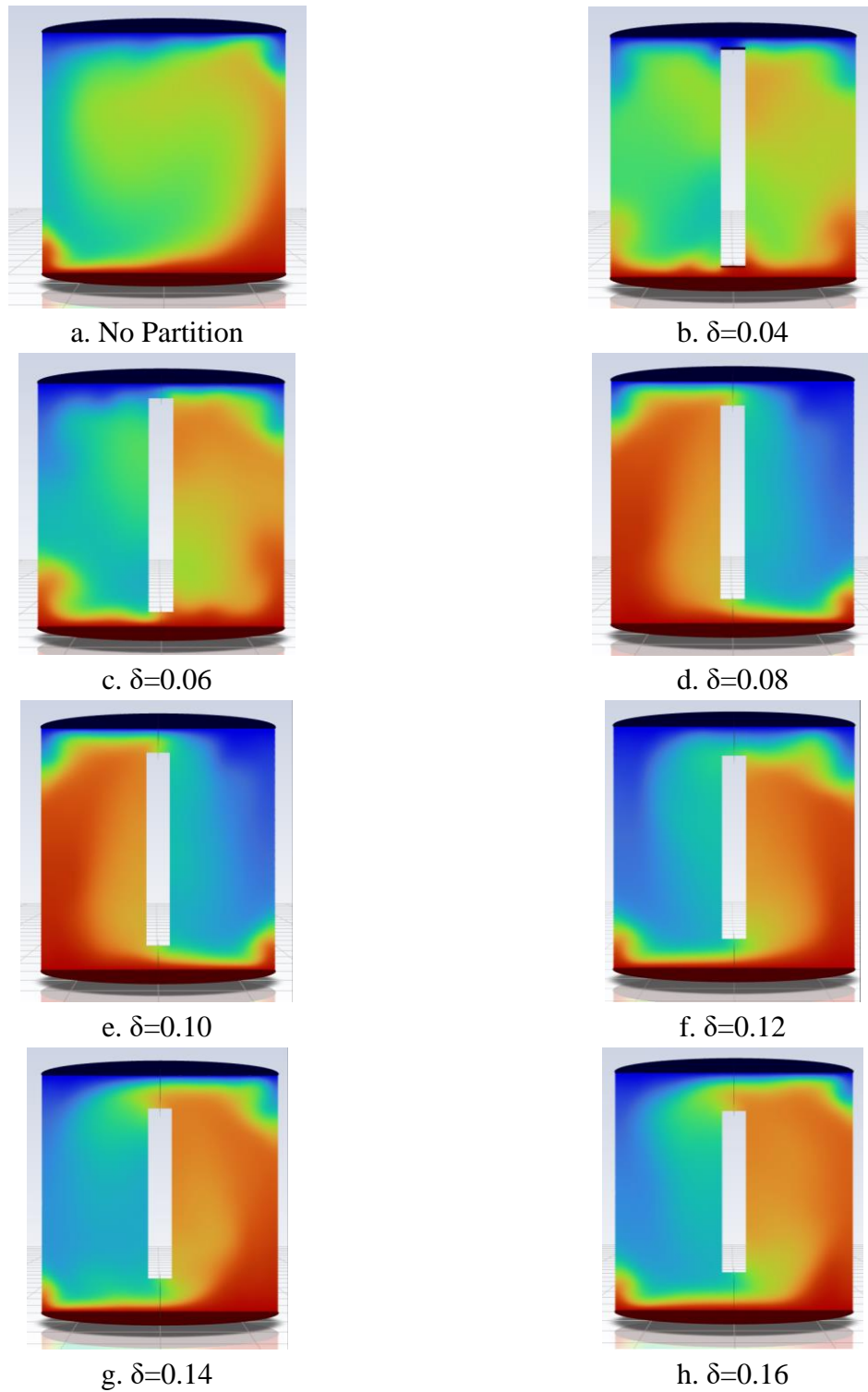
Figure 8. Typical distribution of temperature in the vertical axial cross-section and perpendicular partition. Flows with Ra=10^6, AR=1 are shown.
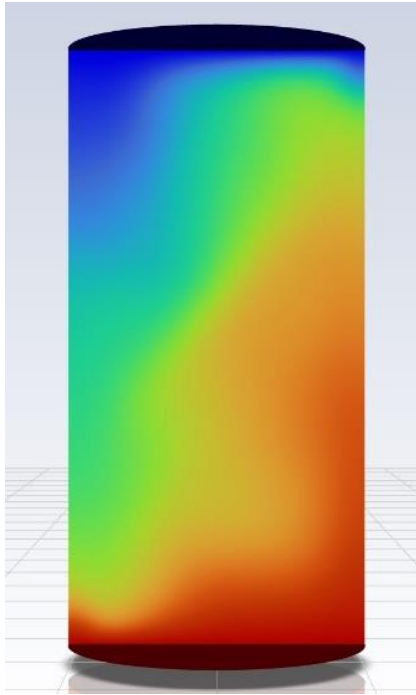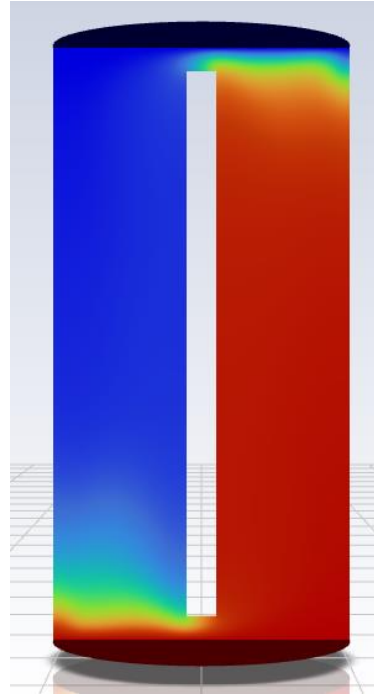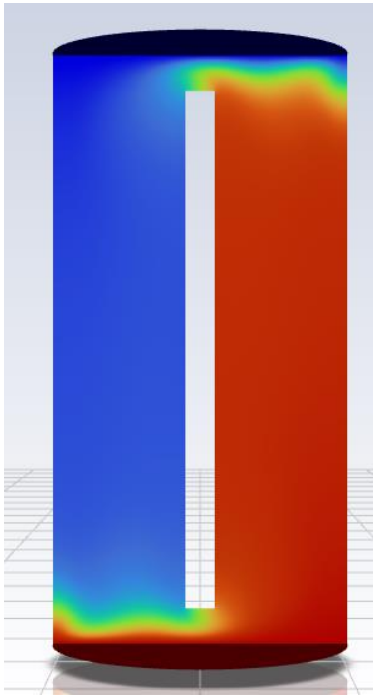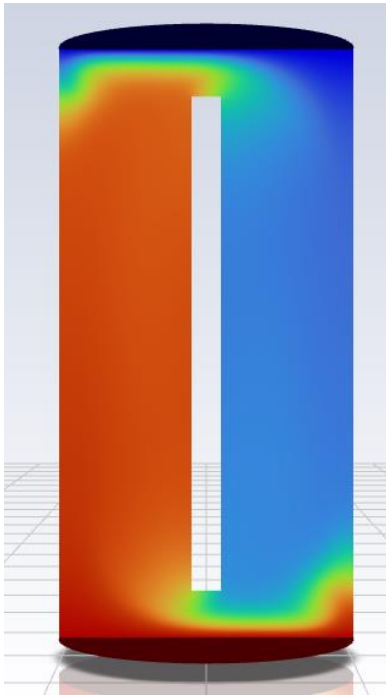
Figure 9. Typical distribution of temperature in the vertical axial cross-section and perpendicular partition. Flows with Ra=10^6, AR=2 are shown.
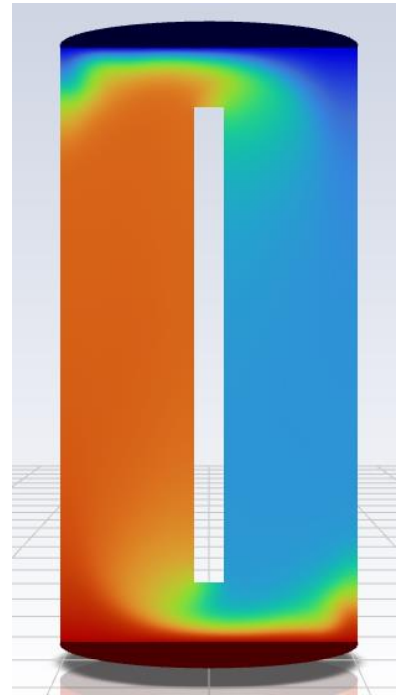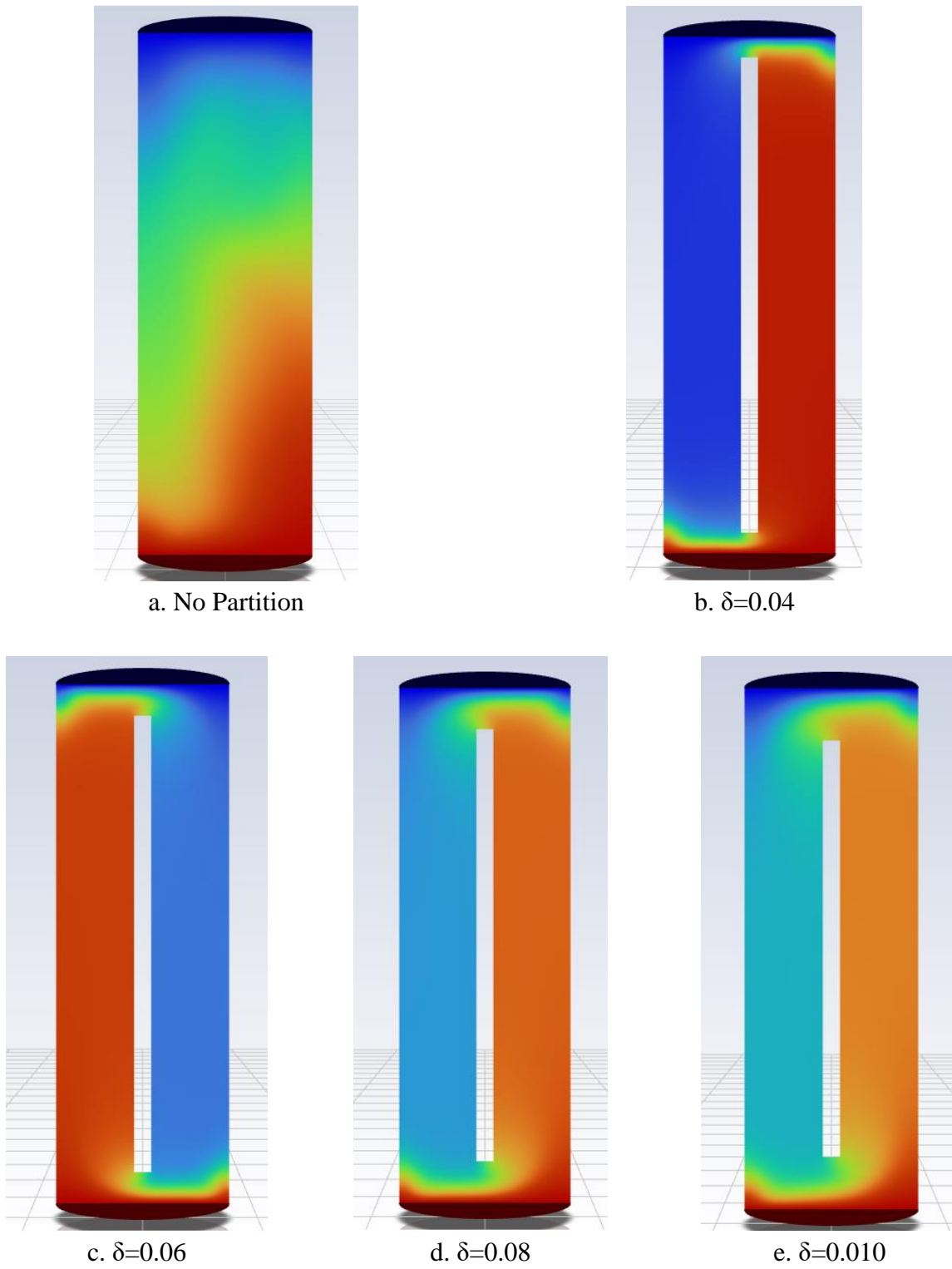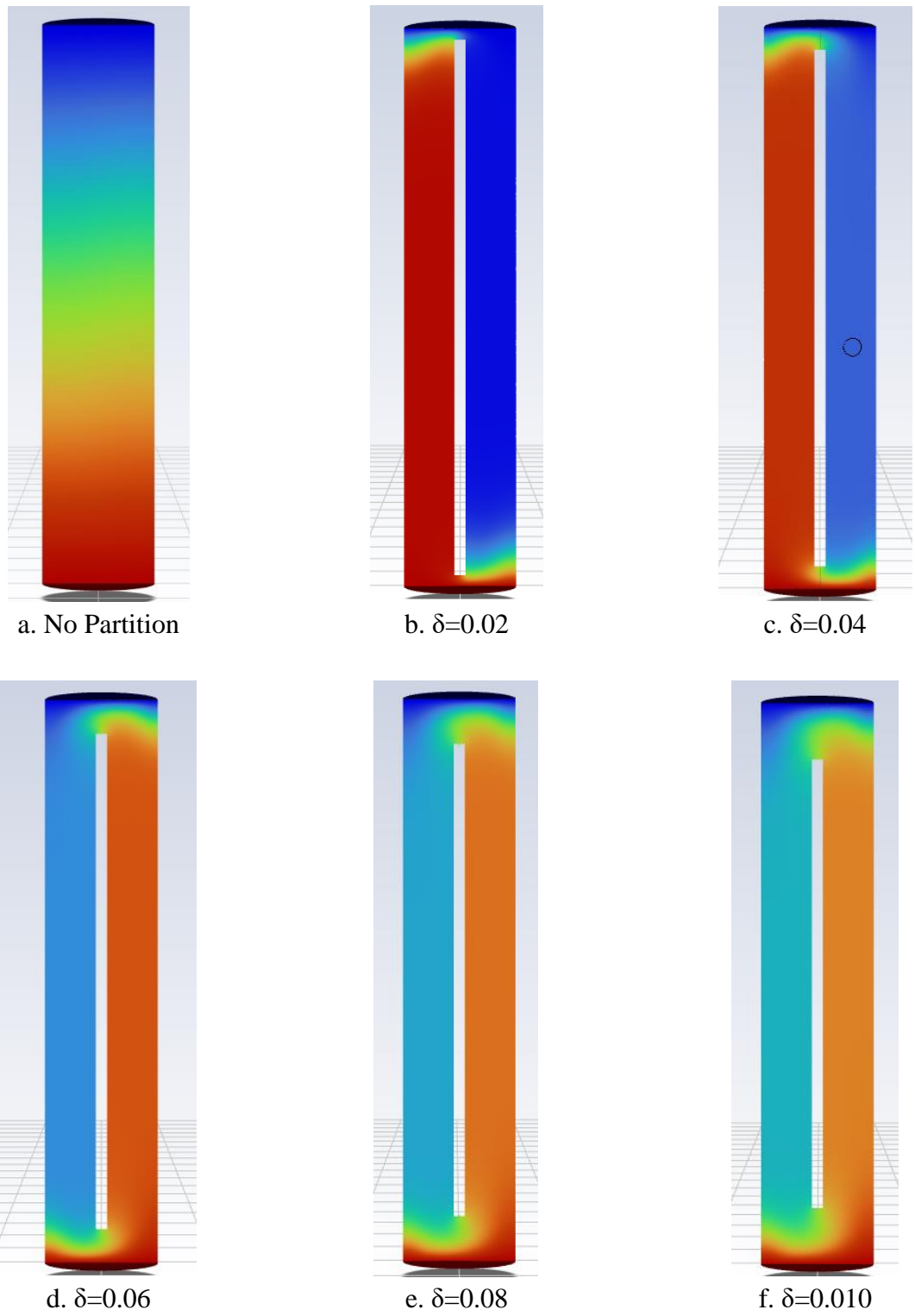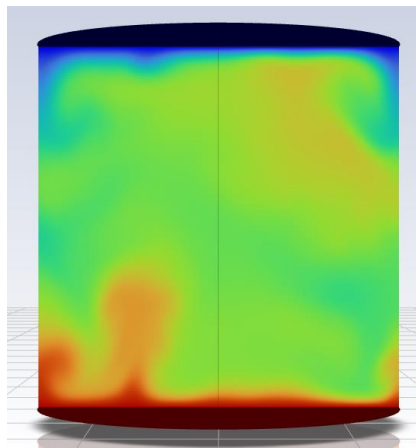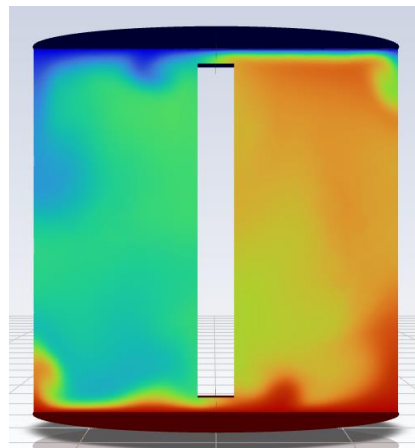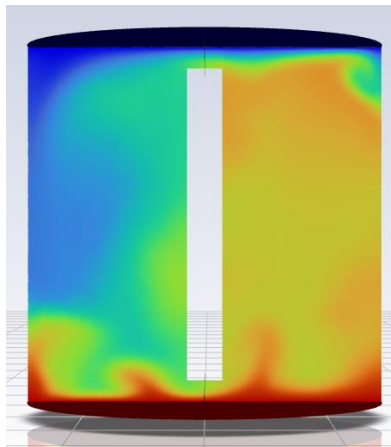
a. No Partition

b. δ=0.04

c. δ=0.06

d. δ=0.08

e. δ=0.010

Figure 10. Typical distribution of temperature in the vertical axial cross-section and

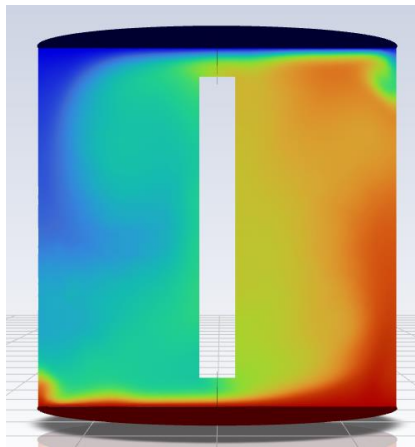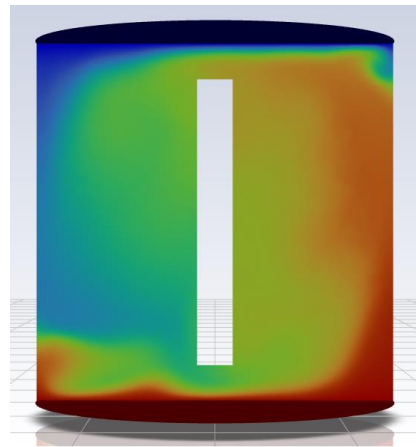perpendicular partition. Flows with Ra=10^6, AR=1 are shown.

a. No Partition   b. δ=0.02   c. δ=0.04

d. δ=0.06   e. δ=0.08   f. δ=0.010

Figure 11. Typical distribution of temperature in the vertical axial cross-section and perpendicular partition. Flows with Ra=10^6, AR=5 are shown.
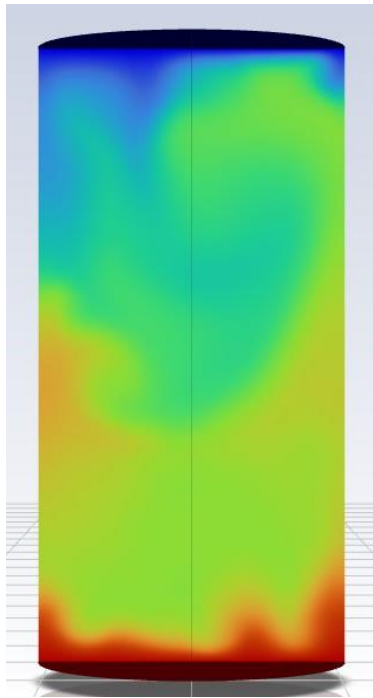
a. No Partition
b. δ=0.04
c. δ=0.06
d. δ=0.08
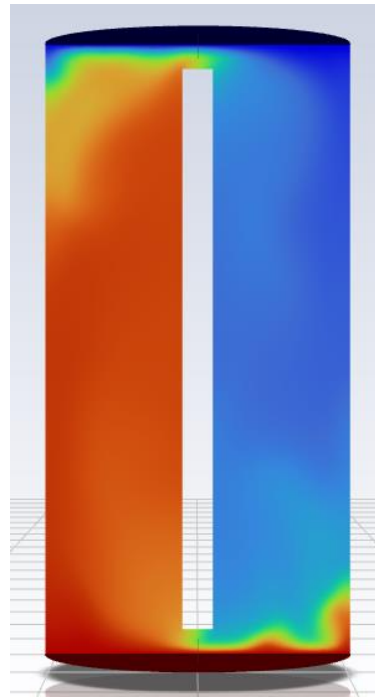e. δ=0.010

Figure 12. Typical distribution of temperature in the vertical axial cross-section and

perpendicular partition. Flows with Ra=10^7, AR=1 are shown.

a. No Partition　　　　　　　　　　　　b. δ=0.04

c. δ=0.06　　　　　　d. δ=0.08　　　　　　e. δ=0.010

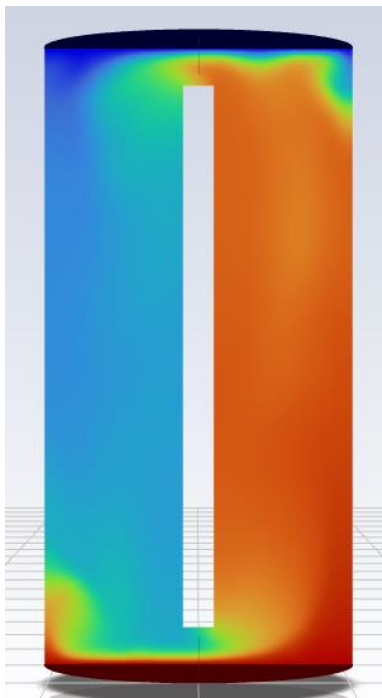Figure 13. Typical distribution of temperature in the vertical axial cross-section and
perpendicular partition. Flows with Ra=10^7, AR=2 are shown.

Figure 14. Typical distribution of temperature in the vertical axial cross-section and perpendicular partition. Flows with Ra=10^7, AR=3 are shown.

a. No Partition   b. δ=0.01   c. δ=0.02

d. δ=0.04   e. δ=0.06   f. δ=0.08   g. δ=0.01

Figure 15. Typical distribution of temperature in the vertical axial cross-section and perpendicular partition. Flows with Ra=10^7, AR=5 are shown.
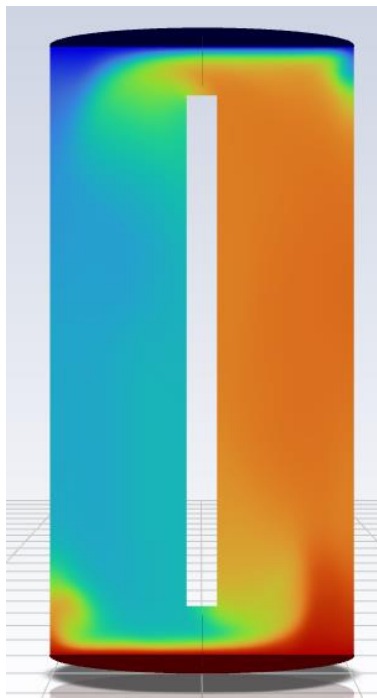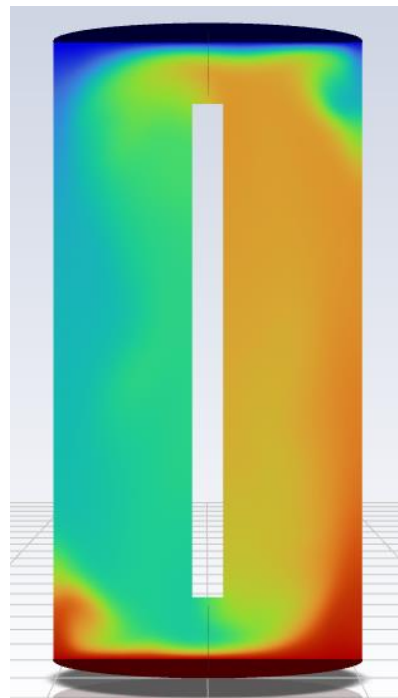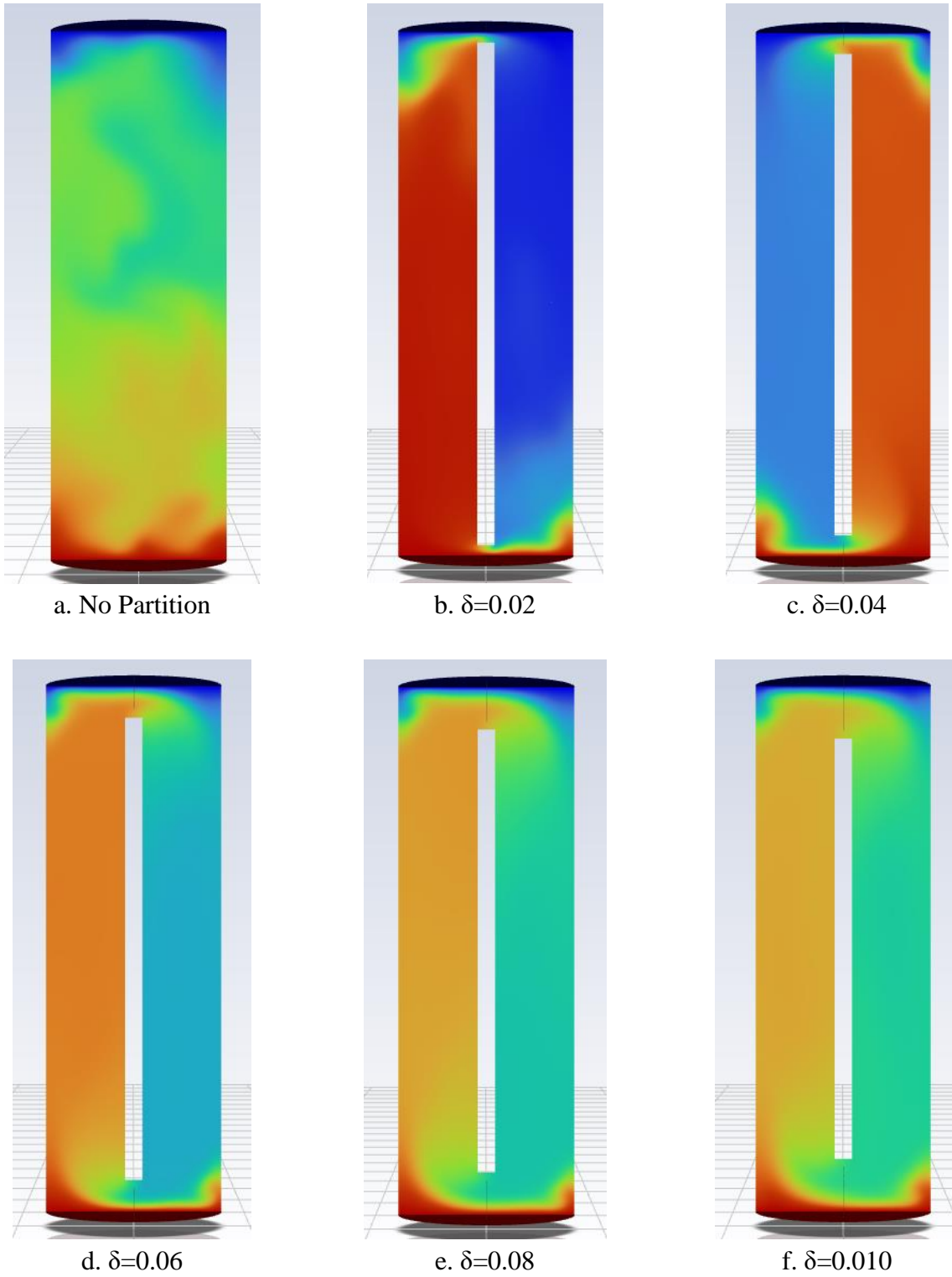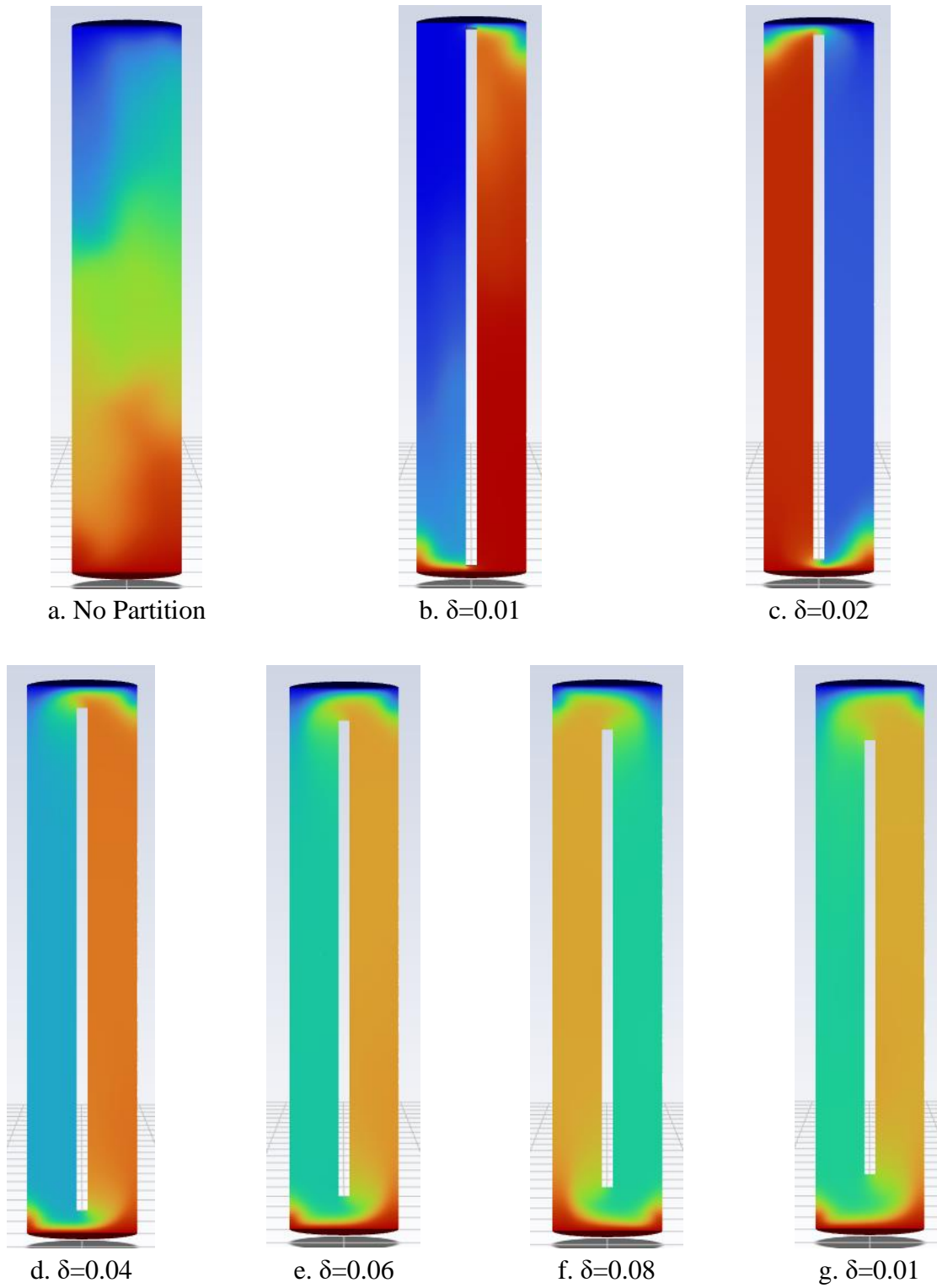
Organization of the flow due to the addition of the partition is evident in the simulation of the temperature and velocity contours shown in Figures 16 and 17. Horizontal jets occur at the top and bottom gaps with the addition of the partition and large-scale circulation is produced. These jets flow through and disrupt the top and bottom thermal boundary layers, contributing to thermal efficiency. Given the results in Table 4, it can be assumed that organization of the fluid flow facilitates increased convective heat transfer. The one instance in which convective heat transfer experienced a decrease in Nu compared to its non-partitioned case may speak to the theory of increased heat transfer due to a more compressed model as this specific instance was set at AR=1 [6]. Table 6 shows the results for the analysis of the thermal boundary layers and can be observed in Figures 18 and 19.

The case of Ra=10^6 AR=5 with no partition is an outlier of the non-partitioned cases having no velocity with no flow having been developed. This can be observed in Figure 11a where the temperature gradient remains perfectly stratified due to the lack of fluid flow. It has been shown through analysis [13] and demonstrated experimentally [14] that flows within cylindrical containers of AR=5 for a fluid at Ra=10^6 have a stability that falls near the Critical Rayleigh Number, Ra_{cr}, the threshold for which convective flow begins to develop. Due to the strong numerical dissipation produced by the finite-volume scheme used by Fluent, it is possible that a weak convective flow just above Ra_{cr} are not captured in simulation. The comparison of analyzed and experimental data presented by Muller, Neumann, and Weber in their work on natural convection in cylindrical cavities [14] shows that a flow with Ra=10^6 AR=5 is weak and non-turbulent. From this, it can be assumed that flow produced at these conditions does not manifest in Fluent simulation, where flow computed in a non-partitioned domain shows zero velocity and only a purely conduction profile of temperature. This is not surprising, considering
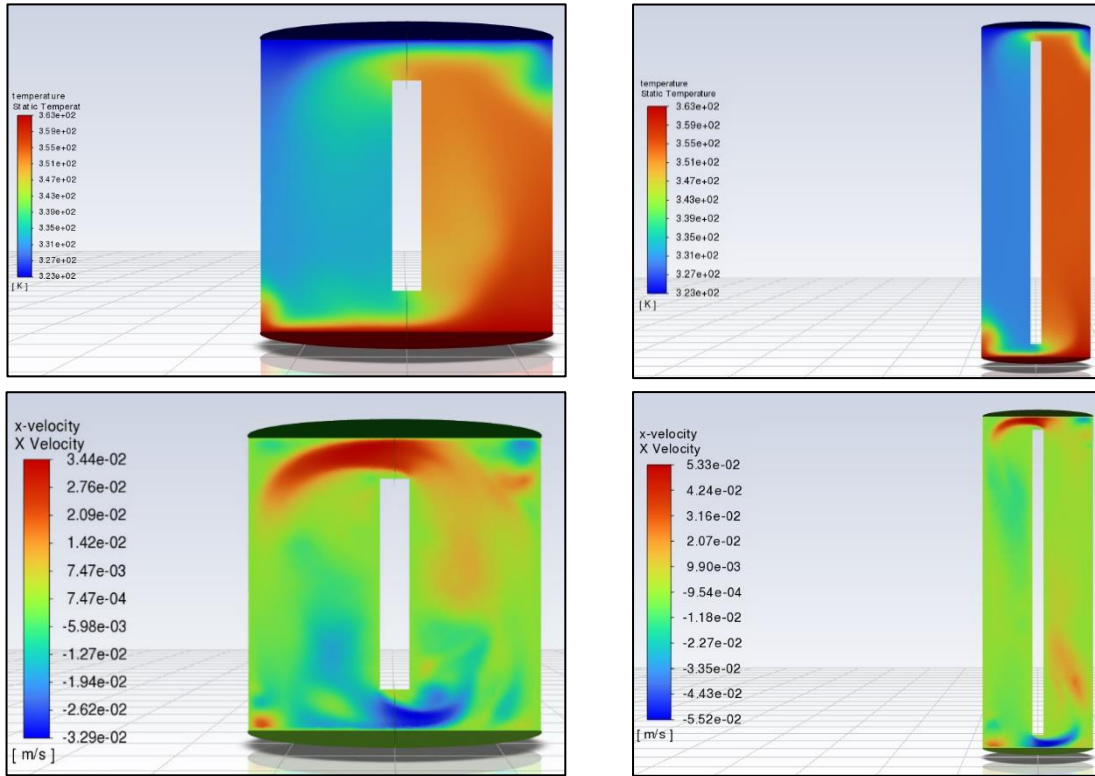
Figure 16. Temperature and velocity contours of x-velocity showing evidence of horizontal jets in the gaps between the top/bottom walls and the partitions. Instantaneous distributions for x-velocity contours Left: Ra=10^6, AR=1, δ=0.14 for nondimensional velocity range -0.74≤u≤0.77; Right: Ra=10^7, AR=3, δ=0.04 for nondimensional velocity range -0.84≤u≤0.81.

Figure 17. Horizontal cross sections of fluid temperature for Ra=10^6, AR=1, and δ=0.14. Left: Cross sections above and below the partition. Right: Cross section through cylinder center.

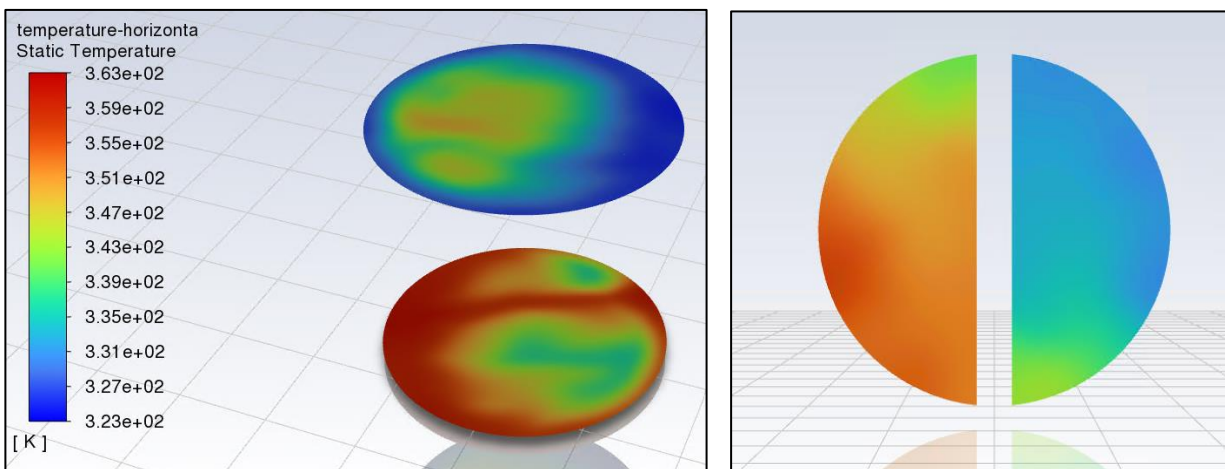that the sidewall closeness increases Ra_{cr} above the point at which convection first occurs, to about $Ra_{cr}=7 \times 10^5$ [14]. Therefore, convection not occurring in the simulations at a slightly higher $Ra=10^6$ is attributable to the known sensitivity of instability to numerical dissipation of the numerical method. The dissipation is relatively high in the finite-volume solution of the models. Results presented in Figure 11 show that a partition may generate convection flow in geometries where convection would not otherwise happen.

3.3. Relation Between the Optimal Gap Size and Thermal Boundary layer Thickness

The relationship between the size of the gaps between the partition and the top and bottom walls and the thickness of the thermal boundary layer is further explored in this section. For calculating the boundary layer thickness, flows computed for non-partitioned domains are used to find the vertical profiles of time-averaged temperature along the cylinder axis. These results are presented in Figures 19 and 20 and show that, except for the case $Ra=10^6$, AR=5, in which no flow and, thus, no boundary layer exists, the boundary layer thicknesses can be determined using (12) and (13) and are shown in Table 7.

The thicknesses obtained in each case for the upper and lower walls are averaged to provide the final estimates for δ_{BL} and presented in Table 7, showing that the boundary layer thickness drops about twofold as Ra increases from 10^6 to 10^7. The effect of AR is weaker. At both values of Ra, δ_{BL} decreases as AR decreases from 1 to 2 and increases with AR at AR ≥ 2. Analysis of the results in terms of the ratio between the partition gap size and the thickness of the thermal boundary layer δ/ δ_{BL} is presented in Figures 20 and 21. Unfortunately, an hypothesis that the amplification of heat transfer can be approximated as a function of the single parameter δ/ δ_{BL} is not supported by the data. The curves of Nu/Nu_0 obtained for various Ra and AR do not collapse into one curve if plotted with δ/ δ_{BL} (see Figure 18). Even more disappointing is that the

ratio δ_{max}/δ_{BL} varies strongly with Ra and AR. The scatter plot of δ_{max} vs δ_{BL} shown in Figure 21 also does not show any clear dependency. However, while the hypothesis that δ_{max}/δ_{BL} being a defining parameter is disproved by the results, it can be concluded that the optimal gap size δ_{max} is always smaller than the boundary layer thickness. This means that the partition must penetrate the thermal boundary layer to facilitate a strong heat transfer enhancement.
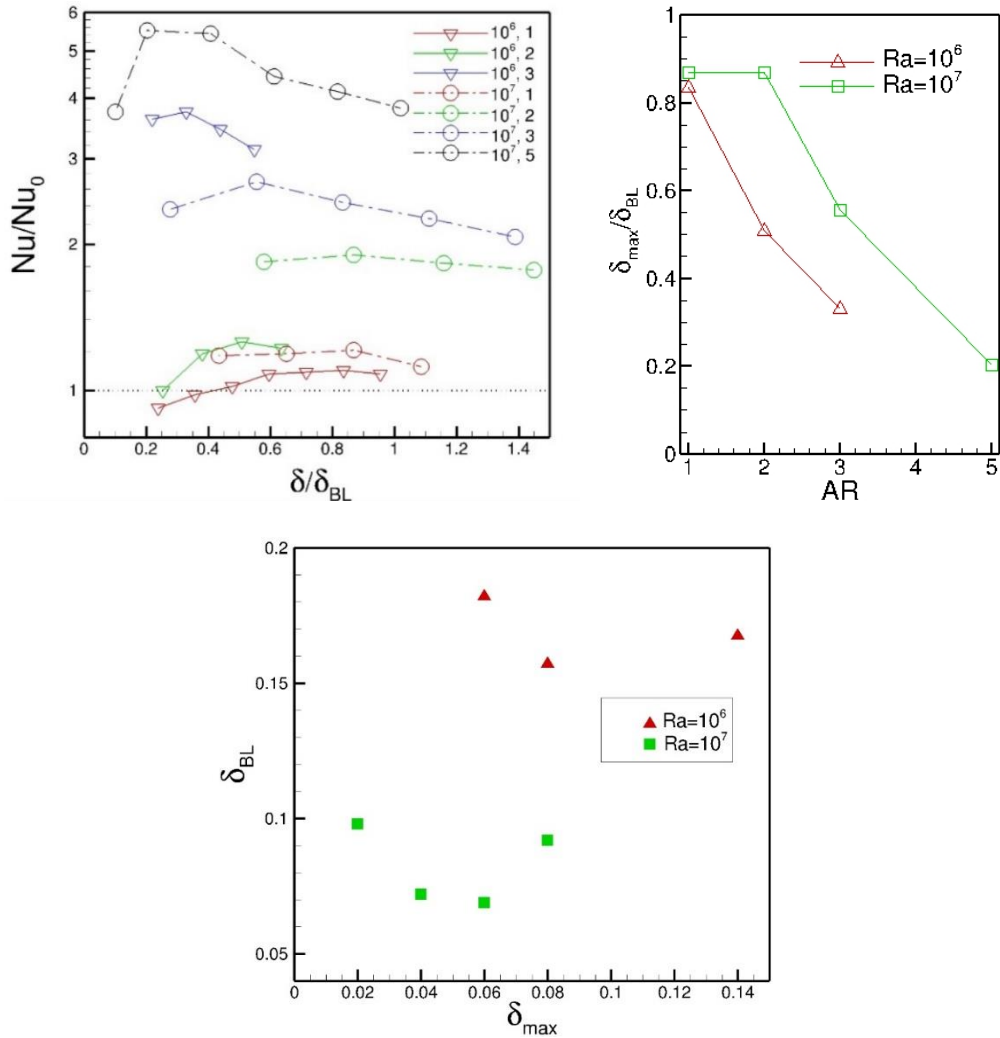
Figure 18. Top Left: Normalized values of the Nusselt number as a function of the single parameter δ/δ_{BL}. Top Right: δ/δ_{BL} as a function of AR (dependence on the geometry of the cylinder). Bottom: Average boundary layer thickness as a function of δ_{max}.

Figure 19. Axial profiles of time-averaged temperature in flows without partitions at Ra=10^6.

Figure 20. Axial profiles of time-averaged temperature in flows without partitions at Ra=10^7.

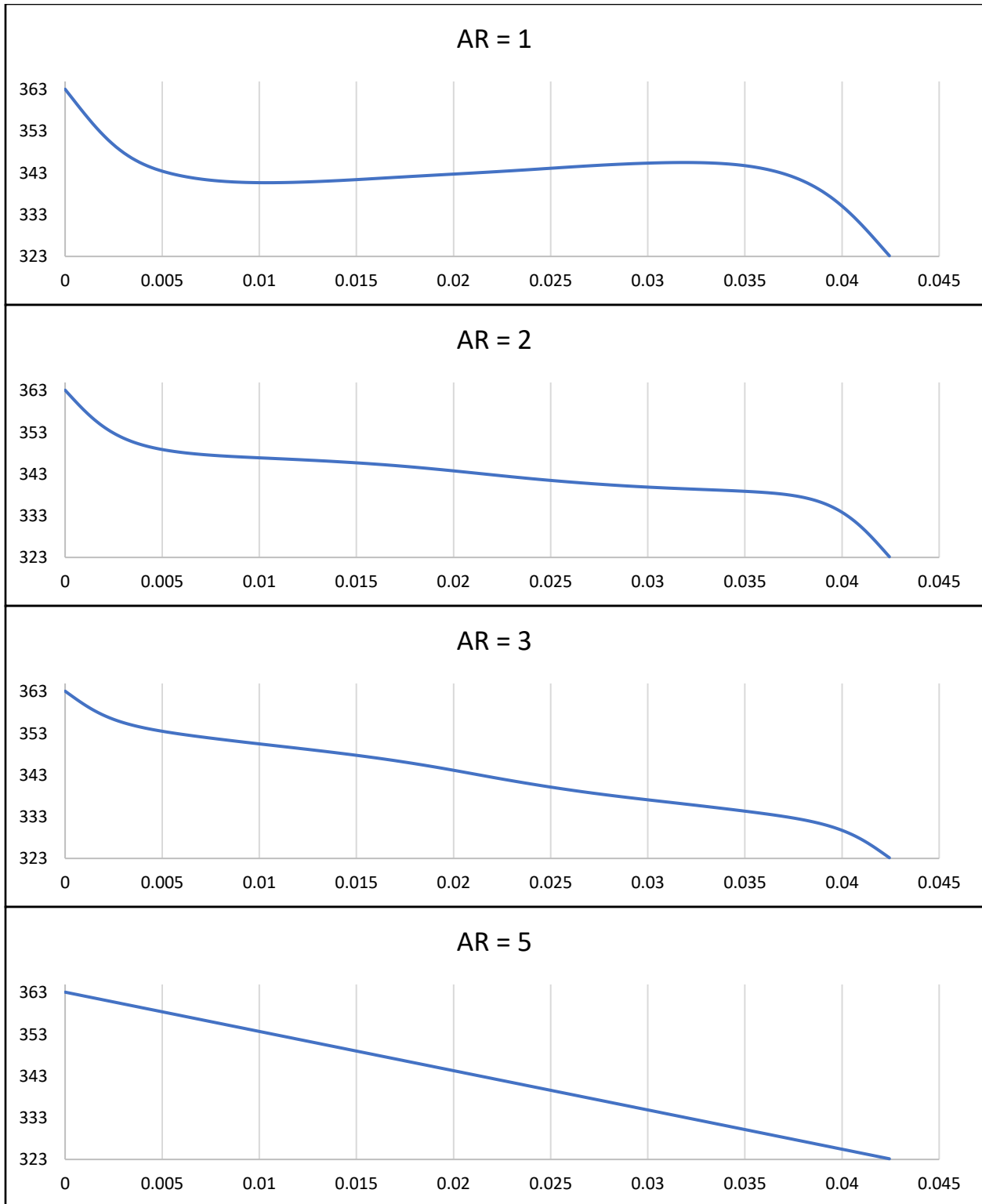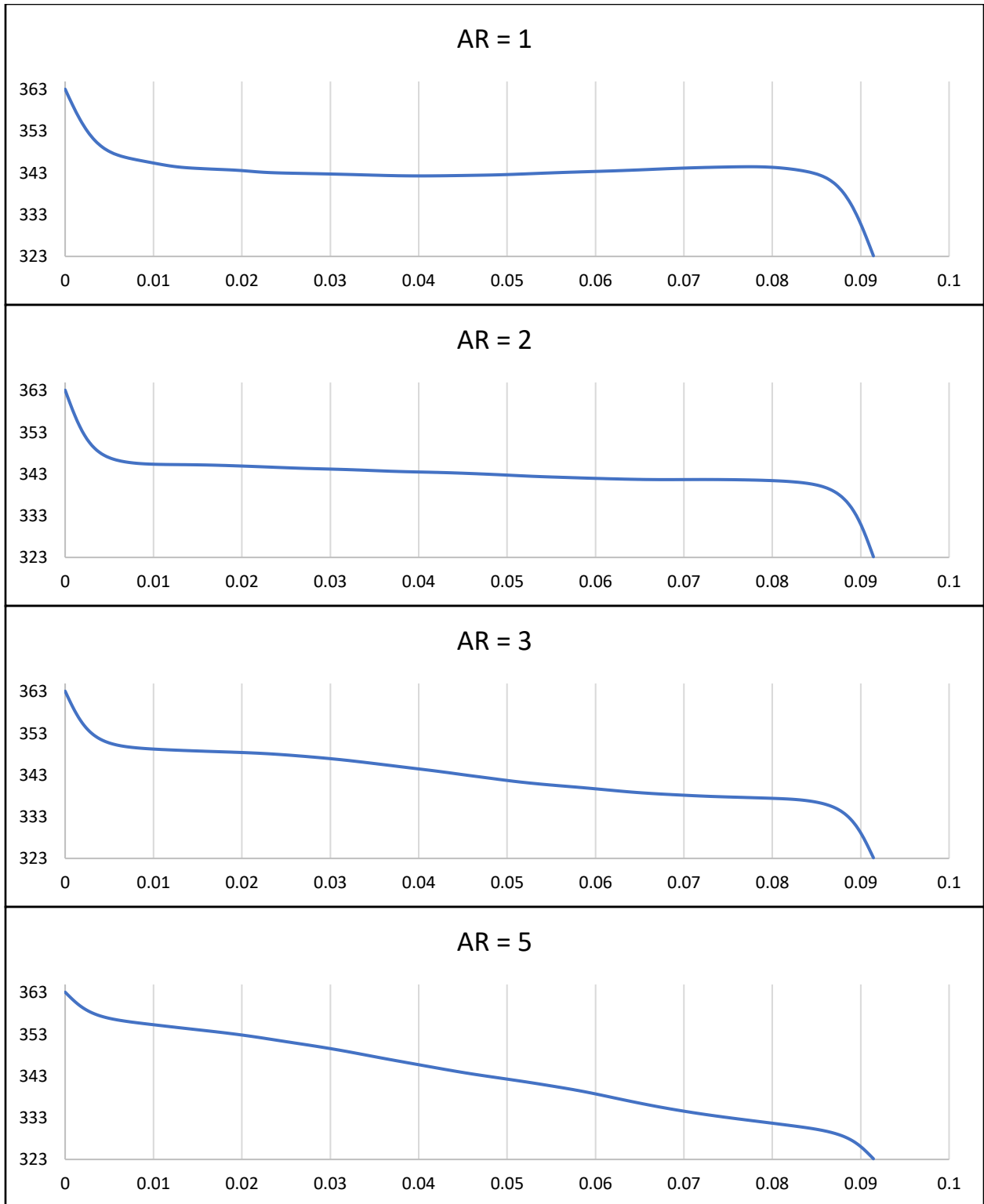| Ra	10^6				10^7			
AR	1	2	3	5	1	2	3	5
T_b	343.08	343.19	343.13	343.15	343.40	343.16	342.90	343.63
$\left\|\frac{dT}{dz}\right\|_{lower}$	2986	2641	1658	N/A	2390	3012	2272	1094
$\delta_{BL,lower}$	6.70	6.52	7.74	N/A	8.08	6.20	6.66	9.07
$\frac{\delta_{BL,lower}}{H}$	0.158	0.154	0.183	N/A	0.088	0.068	0.073	0.099
$\left\|\frac{dT}{dz}\right\|_{upper}$	2660	2549	1686	N/A	2368	2938	2303	1070
$\delta_{BL,upper}$	7.51	6.79	7.70	N/A	8.74	6.43	6.52	8.85
$\frac{\delta_{BL,upper}}{H}$	0.177	0.160	0.181	N/A	0.096	0.070	0.071	0.097
$\frac{\delta_{BL,average}}{H}$	0.167	0.157	0.182	N/A	0.092	0.069	0.072	0.098

Table 7. Thicknesses of the upper and lower thermal boundary layers δ_{BL} (in mm) computed with data from time-averaged temperature fields in domains without partitions (see text for explanations). Note that the mesh refinement zones set in these simulations as 20% of the cylinder height completely cover the thermal boundary layer in all simulations.

3.4. Further Heat Transfer Optimization

In this section, we consider the possible effects of asymmetry between the top and bottom gaps of the partition. The asymmetry is defined by the non-dimensional parameter α, or the ratio of $H_{g,upper}$ and $H_{g,lower}$. A sampling of data was taken for the flow at Ra = 10^6, AR = 1, and δ = 0.06, with α adjusted from 0.5 up to 1.25. A local maximum of the Nusselt number was found at α=0.75.

It was decided to test α=0.75 with the combinations of AR and δ that produced the highest values for Nu at Ra=10^6 and Ra=10^7. The results are presented in Table 8. While there is a similar increase in Nu for optimized conditions at Ra=10^7, there is a slight decrease for Ra=10^6. These findings suggest that there is a potential for further increase of heat transfer rate. Further investigations are required to explore this effect.

Ra	δ	α =0.75	α =1
10^6	0.06	7.00	6.20
10^6	0.14	6.85	6.90
10^7	0.08	14.2	12.8

Table 8. Comparison of Nu as a function of α for set combinations of non-dimensional variables.

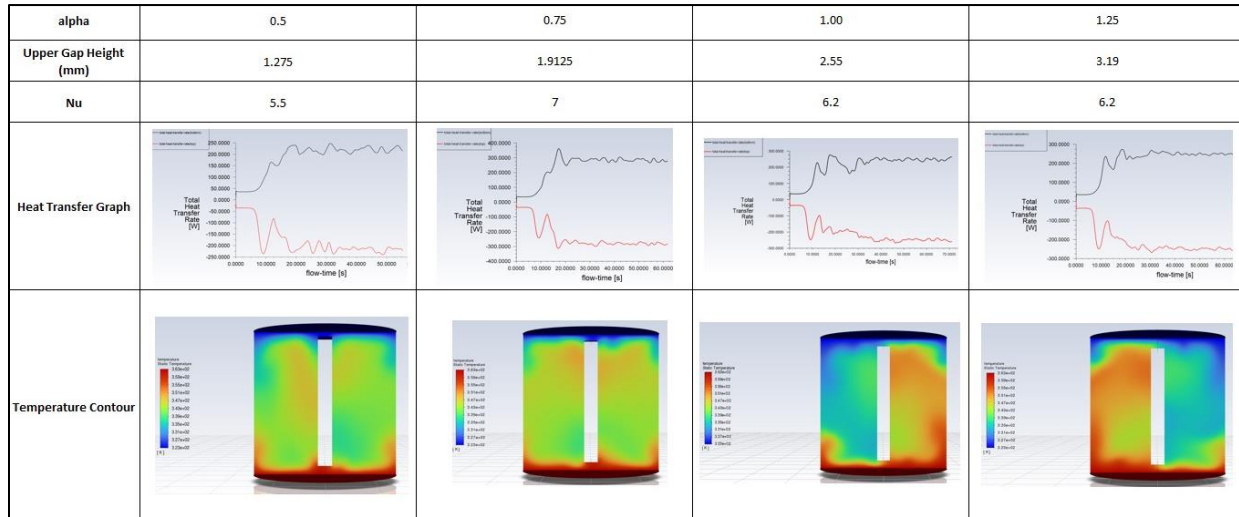| alpha	0.5	0.75	1.00	1.25
Upper Gap Height (mm)	1.275	1.9125	2.55	3.19
Nu	5.5	7	6.2	6.2
Heat Transfer Graph				
Temperature Contour				

Figure 21. Results of modifying α for Ra = 10^6, AR = 1, and δ = 0.06.

4. Conclusion

This thesis presented the results of numerical simulations of the Rayleigh-Benard convection in cylindrical cells with a vertical partition and liquid gallium as a working fluid. The results show that the use of a partition leads to very strong (more than tenfold in one case) amplification of the rate of heat transfer. The amplification is much stronger than what was observed in earlier studies with water [2], [6], [7] which we attribute to the effect of the low Pr of gallium. Moreover, we found that with a configuration close to convection stability limit (Ra=10^6, AR=5) the presence of a partition may cause a convection flow, even while such a flow is not observed in the non-partitioned case. Unfortunately, our hypothesis that the effect of heat transfer amplification is largely determined by the ratio of the gap width between the partition and the cylinder walls and the thickness of the thermal boundary layer was not supported by our data. Nevertheless, it can be concluded that the optimal gap size δ_{max} is always smaller than the boundary layer thickness, meaning the partition penetrating the thermal boundary layer does assist in heat transfer enhancement.

Supplementary exploration of the combined effects studied in this thesis includes extending the analysis to higher Ra, higher and lower AR, and various values of α. Additionally, it is anticipated that the effect of heat transfer enhancement is not limited to the geometry of a cylinder with a single partition. Other cavity shapes (e.g. a cuboid) and the use of multiple partitions may prove beneficial. Lastly, an experiment confirming the effect may be simple enough to perform and would further validate the simulated data.

Future work related to this research may include more accurate numerical simulations, which would be free from numerical dissipation and other accuracy-detrimental features of a commercial CFD model. Furthermore, research into the use of an asymmetrically positioned partition indicates the possibility of additional heat transfer amplification.

The simulated data from this study may prove useful for thermal management of systems in which a significant amount of convective heat transfer is required. An example of this would be a horizontally mounted cpu with a hypothetical cold sink resting above it. A convective cell using a low temperature liquid metal could be used in between to facilitate a large amount of heat transfer from the cpu for cooling [12]. Other promising applications are stationary battery energy storage or cooling for high-rate power electronics equipment. A provision patent application on the use of the described technological innovation is planned for the near future.

References

[1] J. Scheel and J. Schumacher, "Global and local statistics in turbulent convection at low Prandtl numbers," *Journal of Fluid Mechanics*, vol. 802, pp. 147–173, Aug. 2016

[2] Y. Bao, J. Chen, B.-F. Liu, Z. She, J. Zhang, and Q. Zhou, "Enhanced heat transport in partitioned thermal convection," *Journal of Fluid Mechanics*, vol. 784, Nov. 2015

[3] O. Shishkina and S. Horn, "Thermal convection in inclined cylindrical containers," *Journal of Fluid Mechanics*, vol. 790, Feb. 2016

[4] L. Zhang and K. Xia, "Achieving heat transfer enhancement via manipulation of bulk flow structures in turbulent thermal convection," *Physical Review Fluids*, vol. 8, no. 2, Feb. 2023

[5] L. Yuan, S. Zou, Y. Yang, and S. Chen, "Boundary-Layer disruption and Heat-Transfer enhancement in convection turbulence by oscillating deformations of boundary," *Physical Review Letters*, vol. 130, no. 20, May 2023

[6] S. Di Huang, M. Kaczorowski, R. Ni, and K. Xia, "Confinement-Induced Heat-Transport enhancement in turbulent thermal convection," *Physical Review Letters*, vol. 111, no. 10, Sep. 2013

[7] J. Chen, Y. Bao, Z. Yin, and Z. She, "Theoretical and numerical study of enhanced heat transfer in partitioned thermal convection," *International Journal of Heat and Mass Transfer*, vol. 115, pp. 556–569, Dec. 2017

[8] P. K. Kar, U. Chetan, J. Mahato, T. L. Sahu, P. K. Das, and R. Lakkaraju, "Heat flux enhancement by regular surface protrusion in partitioned thermal convection," *Physics of Fluids*, vol. 34, no. 12, Dec. 2022

[9] O. Zikanov, I. A. Belyaev, Y. Listratov, P. Frick, N. G. Razuvanov, and V. G. Sviridov, "Mixed convection in pipe and duct flows with strong magnetic fields," *Applied Mechanics Reviews*, vol. 73, no. 1, Jan. 2021

[10] O. Zikanov, *Essential computational fluid dynamics*, 2nd Edition. John Wiley & Sons, 2019.

[11] Y. Cengel, R. Turner, and J. Cimbala, *Fundamentals of thermal-fluid sciences*, 4th Edition. McGraw-Hill, 2012.

[12] J. Liu, *Advanced liquid metal cooling for chip, device and system*. 2022.

[13] G. S. Charlson and R. L. Sani, "On Thermoconvective instability in a bounded cylindrical fluid layer," *International Journal of Heat and Mass Transfer*, vol. 13, no. 9, pp. 1479–1496, Sep. 1970

[14] G. Müller, G. Neumann, and W. Weber, "Natural convection in vertical Bridgman configurations," *Journal of Crystal Growth*, vol. 70, no. 1–2, pp. 78–93, Dec. 1984